Axisymmetric Eigenmodes of Spheroidal Pure Electron Plasmas

Yosuke KAWAI*, Jun AOKI† and Yasuhito KIWAMOTO‡

Graduate school of Human and Environmental Studies, Kyoto University, Yoshida Nihonmatsu-cho, Sakyo-ku, Kyoto 606-8501, Japan

(Received 17 December 2009 / Accepted 6 May 2010)

The axisymmetric electrostatic eigenmodes of spheroidal pure electron plasmas have been studied experimentally. It is confirmed that the observed spheroidal plasma attains a theoretically expected equilibrium density distribution, with the exception of a low-density distribution surrounding the plasma. When the eigenmode frequency observed for the plasma is compared with the frequency predicted by the dispersion relation derived under the assumption of ideal conditions wherein the temperature is zero and the boundary is located at an infinite distance from the plasma, it is observed that the absolute value of the observed frequency is systematically higher than the theoretical prediction. Experimental examinations and numerical calculations indicate that the finite temperature effect alone cannot account for the upward shift of the eigenmode frequency, which is significantly affected by image charges induced on the conducting boundary.

Keywords: nonneutral plasma, electrostatic wave and oscillation

DOI: 10.1585/pfr.5.S2038

1. Introduction

A non-neutral plasma in a homogeneous magnetic field $\boldsymbol{B} = B_0\hat{z}$ and a harmonic electrostatic potential well is theoretically predicted to evolve to thermal equilibrium in the form of a rigidly rotating spheroid of uniform density [1]. The dispersion relation for the electrostatic eigenmodes of a spheroidal plasma can be determined analytically to be dependent on the plasma density and the the aspect ratio (that is the ratio between axial and radial extents of the spheroidal plasma) [2]. This property of the eigenmodes has been examined experimentally with pure ion plasmas or pure electron plasmas [3–6] from the viewpoint of its application to the nondestructive diagnostics of plasma characteristics and, in particular, to measurements of difficult-to-produce species such as positrons [7, 8].

The dispersion relation was derived for a plasma under ideal conditions wherein the temperature is zero and the boundary is located at an infinite distance from the plasma [2]. In practice, however, the actual experimental conditions are often different from the theoretical assumptions, and the effect of the difference on the observed eigenmode properties has not been sufficiently examined in experiments. In this study, we investigate the frequency characteristics of axisymmetric eigenmodes excited in an experimentally observed spheroidal plasma with a wide variety of equilibrium density distributions.

author's e-mail: kawai@ppl.k.u-tokyo.ac.jp

*Present Affiliation: Graduate School of Frontier Sciences, The University of Tokyo, 5-1-5 Kashiwanoha, Kashiwa, Chiba 277-8561, Japan.

†Present Affiliation: Graduate School of Science, Osaka University, Toyonaka-shi, Osaka, 560-0043, Japan.

‡Present Affiliation: Professor Emeritus at Kyoto University

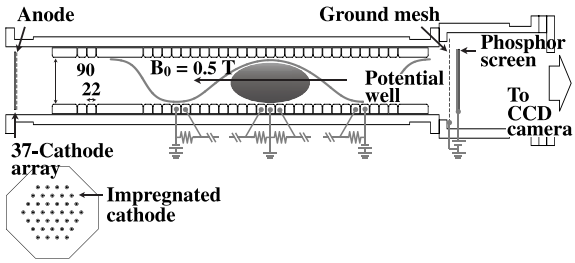

Fig. 1 Schematic view of experimental configuration.

2. Experimental Setup and Method

The experiment is carried out using a pure electron plasma trapped in a Penning trap with a uniform magnetic field ($B_0 = 0.5$ T) and a harmonic potential well, as shown schematically in Fig. 1. The conducting wall of radius $R_W = 45$ mm consists of ring electrodes axially aligned with a pitch of 24 mm. By assigning a stepwise voltage to each electrode, a harmonic potential distribution is formed in the central region of the trap [6, 9]. From preselected cathode elements, electrons are introduced into the trap through a temporally decreased potential barrier at one end of the harmonic well. After several seconds of isolated relaxation following repetitive operations of an injection-hold cycle, the electron density distribution evolves to an axisymmetric single-peak profile.

Axisymmetric eigenmodes are resonantly excited by applying a burst of rf perturbations to one electrode at a frequency that is linearly ramped up from 4 to 20 MHz over a period of 30 ms. The excited mode is detected through image charges induced by the plasma motion on another

electrode. The axial mode number ℓ is directly identified by observing the phase differences among the wave signals detected on each electrode.

After the eigenmode is detected, by removing one side of the potential barrier, the electrons are dumped onto the conducting phosphor screen biased at 5 kV, and the resultant luminosity distribution is recorded with a charge-coupled-device (CCD) camera. The conducting screen also serves as an electron collector to determine the number of trapped electrons. Because the total electron number is confirmed to be linearly related to the integrated luminosity of the CCD image, the luminosity distribution provides an absolute measurement of the line-density distribution integrated along the magnetic field lines [10].

The three-dimensional (3D) distribution of the electron density $n(r, z)$ is obtained from the observed line-integrated density profile $n_\ell(r)$ by solving the Boltzmann-Poisson equation [9]

$$\nabla^2\phi^{\mathrm{S}}(r,z) = \frac{e}{\varepsilon_0}n(r,z) = \frac{e}{\varepsilon_0}n_\ell(r)\frac{\exp\left[(\phi^{\mathrm{T}}+\phi^{\mathrm{S}})/T_{\mathrm{e}}\right]}{\int \mathrm{d}z \exp\left[(\phi^{\mathrm{T}}+\phi^{\mathrm{S}})/T_{\mathrm{e}}\right]}, \quad (1)$$

where ϕ^{T}, ϕ^{S}, T_{e}, $-e$, and ε_0 are the trap potential, self-field potential, electron temperature, electron charge, and dielectric constant in vacuum, respectively. Here, it is assumed that T_{e} is spatially homogeneous and that the plasma is in local thermal equilibrium along each magnetic field line, so that the density at each radius has a Boltzmann distribution. The density distribution $n(r, z)$ is determined under the condition $\int \mathrm{d}z n(r, z) = n_\ell(r)$ that is imposed by the experimental observation of the line-density profile $n_\ell(r)$ [9]. The electron temperature is determined by analyzing a radial profile of electrons escaping over the slightly lowered potential battier [9]. The typical temperature in this experiment is evaluated to be $T_{\mathrm{e}} \leq 0.1$ eV.

An example of the 3D density distribution $n(r, z)$ thus obtained is shown in Fig. 2. Figure 2 (a) shows the line-integrated density profile $n_\ell(r)$ obtained by azimuthally averaging a 2D luminosity distribution (Fig. 2 (a), inset). By solving Eq. (1) using the measured $n_\ell(r)$ and $T_{\mathrm{e}} \approx 0.1$ eV, the 3D distributions of the density $n(r, z)$ and the self-consistent potential $\phi^{\mathrm{S}}(r, z)$ are obtained. The contour plots of the resultant $n(r, z)$ and the total potential distribution $(\phi^{\mathrm{T}} + \phi^{\mathrm{S}})(r, z)$ are shown in Fig. 2 (b), and the radial and axial density profiles are shown in Figs. 2 (c) and (d), respectively. The function $n(r, z)$ is ellipsoidal, and inside the plasma, the density is nearly uniform with a sharp boundary in the axial direction. Furthermore, the total potential is almost constant along the magnetic field line. These observations are consistent with the theoretical expectations for a plasma in thermal equilibrium [1]. However, on account of a halo distribution surrounding the plasma, the radial density distribution differs from a stepwise profile and extends to the conducting wall. In this example, the estimated plasma parameters are radius $r_{\mathrm{p}} \approx 9.4$ mm, semi-

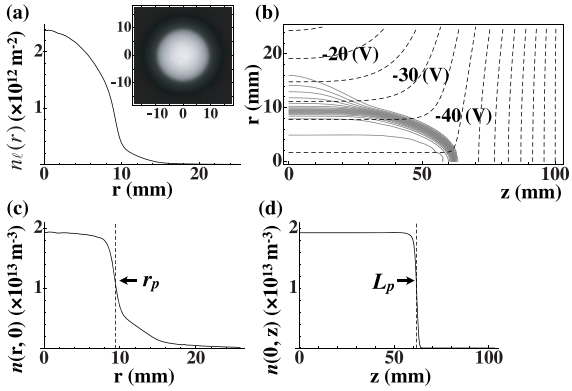

Fig. 2 Example of a 3D density distribution $n(r, z)$. (a) Line-integrated density profile $n_\ell(r)$ obtained by azimuthally averaging a 2D luminosity distribution (inset). (b) Contour plots of $n(r, z)$ (solid line) and total potential distribution $(\phi^{\mathrm{T}} + \phi^{\mathrm{S}})(r, z)$ (dashed line) obtained by solving Eq. (1) using $n_\ell(r)$. (c) Radial density profile $n(r, 0)$. (d) Axial density profile $n(0, z)$.

axial length $L_{\mathrm{p}} \approx 62$ mm, aspect ratio α $(= L_{\mathrm{p}}/r_{\mathrm{p}}) \approx 6.6$, and density $n_0 \approx 1.9 \times 10^{13}$ m^{-3}.

3. Thermal Equilibrium

Figure 2 indicates that the observed plasma is consistent with the theoretical thermal equilibrium distribution, with the exception of the halo distribution. In thermal equilibrium under ideal conditions wherein the temperature is zero and the conducting wall is located at an infinite distance from the plasma [1], the density n_0 of a spheroidal plasma confined in a harmonic potential well

$$\phi^{\mathrm{T}}(r,z) = -\frac{m_{\mathrm{e}}\omega_z^2}{4e}\left(z^2 - \frac{r^2}{2}\right),$$

(where m_{e} is the electron mass) is related to the aspect ratio α by the equation

$$\frac{\omega_{\mathrm{p}}^2}{\omega_z^2} = \frac{2}{A_3(\alpha)}. \quad (2)$$

Here, $A_3(\alpha) = 2Q_1[\alpha(\alpha^2-1)^{-1/2}]/(\alpha^2-1)$ (Q_1 is a Legendre function of the second kind), $\omega_{\mathrm{p}} = (e^2 n_0/\varepsilon_0 m_{\mathrm{e}})^{1/2}$ is the plasma frequency, and ω_z is the frequency of a simple harmonic oscillation in the potential well. Moreover, n_0 is related to the rotation frequency ω_{r} of the spheroid [1] as

$$\omega_{\mathrm{p}}^2 = 2\omega_{\mathrm{r}}(\Omega_{\mathrm{c}} - \omega_{\mathrm{r}}), \quad (3)$$

where $\Omega_{\mathrm{c}} = eB_0/m_{\mathrm{e}}$ is the cyclotron frequency.

In Fig. 3, the experimental data is compared with the equilibrium relationships given by Eqs. (2) and (3). Here, we estimate ω_z from the frequency of the detected dipole mode (i.e., the eigenmode with the axial mode number $\ell = 1$) and evaluate ω_{r} as the $\boldsymbol{E} \times \boldsymbol{B}$ drift frequency

$$\omega_{\mathrm{r}} = -\frac{1}{r}\frac{1}{B_0}\frac{\partial(\phi^{\mathrm{T}}+\phi^{\mathrm{S}})}{\partial r},$$

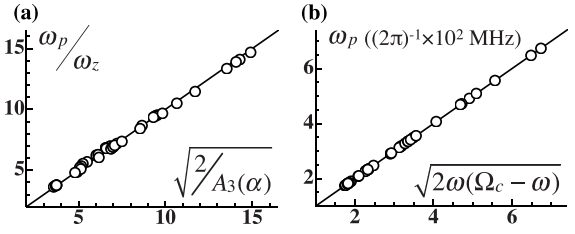

Fig. 3 Comparison between the experimental data and the equilibrium relationships given by Eq. (2) (a) and Eq. (3) (b). The ordinate corresponds to the left-hand-side terms of the equations, and the abscissa indicates the right-hand-side terms.

with the self-field potential ϕ^S obtained from Eq. (1). We find that the observed plasma reasonably satisfies these two relations. This result confirms that the electron plasma observed in this experiment attains the theoretically expected thermal equilibrium state.

4. Eigenmode

The frequency characteristics of the axisymmetric electrostatic eigenmode of the spheroidal plasma are predicted from the dispersion relation [2]

$$1-\frac{\omega_p^2}{\omega_\ell^2}=\frac{k_2}{k_1}\frac{P_\ell(k_1)Q'_\ell(k_2)}{P'_\ell(k_1)Q_\ell(k_2)}, \tag{4}$$

where $k_1=\alpha(\alpha^2-1+\omega_p^2/\omega_\ell^2)^{-1/2}$ and $k_2=\alpha(\alpha^2-1)^{-1/2}$. ω_ℓ indicates the eigenmode frequency of the axial mode number ℓ. The dipole mode $\ell=1$ is a simple harmonic oscillation of the whole plasma in the potential well, so that $\omega_1=\omega_z$. The quadrupole mode $\ell=2$ is an oscillation where the plasma length repeatedly expands and contracts [2, 5].

In Fig. 4, the observed mode frequencies ω_ℓ are plotted as a function of the aspect ratio α for axial mode numbers ℓ from 2 to 6. The frequency is normalized by the dipole mode frequency ω_1 ($=\omega_z$), and the dispersion relation Eq. (2) is denoted by the solid line. As shown in Fig. 4, the dependence on α of the frequency of each mode is similar to the predicted dependence in that the mode frequency increases with α. However, the observed frequencies are systematically higher than the theoretical predictions.

The dispersion relation given by Eq. (4) was derived under the assumption of ideal conditions wherein the temperature is zero and the effect of image charges induced on the conducting wall is negligible [2]. Hereinafter, the discussion focuses on the effect of the finite temperature and of the image charges on the eigenmode frequency. As the analysis of the eigenmode frequency of the axial mode number $\ell>2$ is confirmed to yield results similar to those of the $\ell=2$ mode, the following results are shown only for the quadrupole mode.

4.1 Finite temperature effect

A warm-fluid model predicts an upward shift of the quadrupole mode frequency ω_2^h on account of the increase in the plasma temperature as follows [11]:

$$(\omega_2^h)^2=(\omega_2^c)^2+\frac{5eT_e}{m_eL_p^2}\left(\gamma-\frac{\alpha^2}{2}\left(\frac{\omega_p}{\omega_2^c}\right)^2\frac{d^2A_3(\alpha)}{d\alpha^2}\right), \tag{5}$$

where $\gamma=3$ is the ratio of the specific heats for one-dimensional expansions and ω_2^c is the cold-fluid result determined by Eq. (4). The last term in Eq. (5) describes the frequency shift in terms of the temperature dependence of the plasma shape. If this term is neglected, one obtains a equation similar to the Bohm-Gross dispersion relation $\omega^2=\omega_p^2+\gamma k_z^2eT_e/m_e$ with the parallel wave number $k_z\approx\pi(\ell-1)/2L_p$ [5].

In Fig. 5, we compare the frequency shift $\Delta f_{th}=(2\pi)^{-1}(\omega_2^h-\omega_2^c)$, which is predicted by substituting the measured electron temperature T_e in Eq. (5), and the frequency difference Δf_{ex} between the observed frequency and ω_2^c. The error bars reflect the ambiguity in the measured value of the temperature. The result shows that Δf_{ex} is more than one order of magnitude larger than Δf_{th}.

Figure 6 shows the upward shift of the quadrupole mode frequency with increasing electron temperature. The temperature is raised from 0.1 to 1.4 eV by applying a

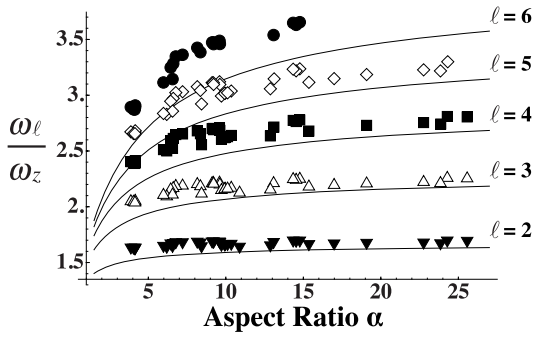

Fig. 4 Comparison between the observed (symbols) and theoretically predicted (solid lines) eigenmode frequencies. The frequencies at axial mode numbers $\ell=2$ (▼), 3 (△), 4 (■), 5 (◊), and 6 (●) are normalized by ω_z and plotted as a function of α.

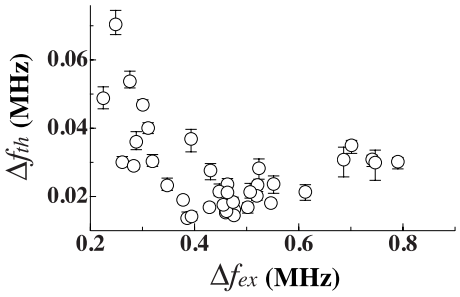

Fig. 5 Comparison between the frequency shift on account of the plasma temperature Δf_{th} predicted from Eq. (5) and the frequency difference Δf_{ex} between the observed frequency and ω_2^c.

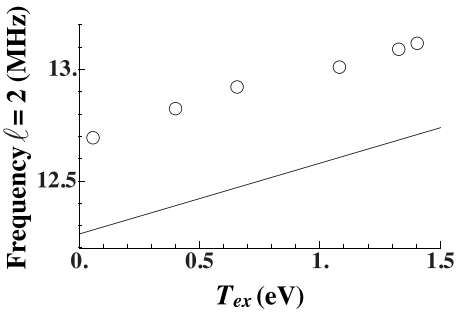

Fig. 6 Dependence of the quadrupole mode frequency on the electron temperature. The open circles indicate the observed frequency and the solid line corresponds to the theoretical prediction given by Eq. (5).

square wave to one end of the trap potential, thereby adiabatically compressing and expanding the plasma in the axial direction repeatedly [12]. The rate of increase in the observed frequency is consistent with the theoretical prediction given by Eq. (5), but there remains a systematic difference of around 0.3 MHz between the observed and predicted frequencies, which is converted to $T_e = 0.8$ eV using Eq. (5).

These observations demonstrate that the discrepancy between the observed and predicted mode frequencies cannot be accounted for only by the finite temperature effect.

4.2 Image charge effect

In order to investigate the effect of image charges on mode frequency, correlations are made between the ratio of the observed frequency ω_2^{ex} to the frequency ω_2^{th} theoretically predicted using Eq. (4) and the plasma parameters α, r_p, L_p, and the total electron number N_p. The result is shown in Fig. 7. The symbols ▼ and ■ correspond to $\alpha \approx 6.5$ and 9.6, respectively. Although the aspect ratio is nearly constant (see ▼ and ■ in Fig. 7 (a)), the ratio $\omega_2^{ex}/\omega_2^{th}$ increases with r_p, L_p, and N_p, i.e., the mode frequency shifts upward with increasing plasma size. As the plasma expands and approaches the conducting wall, the effect of image charges induced on the wall becomes increasingly significant. Therefore, this observation indicates that the mode frequency increases on account of the image charge effect.

To verify this result, we numerically calculated the variation in the mode frequency as a function of the position of the conducting wall using a particle-in-cell simulation [5, 13]. For each wall position, the initial density distributions were obtained by solving Eq. (1) with the common harmonic trap potential $\phi^T(r, z)$ and line-density profile $n_\ell(r)$. The dipole and quadrupole modes were excited by displacing all the particles along the same axial direction and by stretching the plasma along the magnetic field line. The plasma parameters were set as $r_p \approx 6$ mm, $L_p \approx 49$ mm, $\alpha \approx 8$, and $T_e = 0.1$ eV. The frequencies of the dipole and quadrupole modes were measured by using a least-square sinusoidal fit to the time evolution of the center-of-mass position and the plasma length.

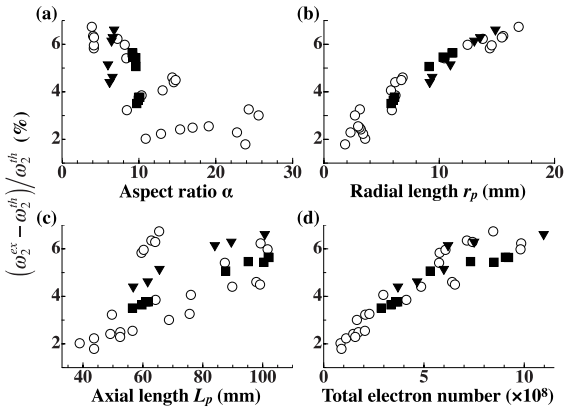

Fig. 7 Correlations between the ratio of the observed frequency ω_2^{ex} to the frequency ω_2^{th} theoretically predicted using Eq. (4) and the plasma parameters (a) α, (b) r_p, (c) L_p, and (d) the total electron number N_p. The symbols ▼ and ■ correspond to $\alpha \approx 6.5$ and 9.6, respectively.

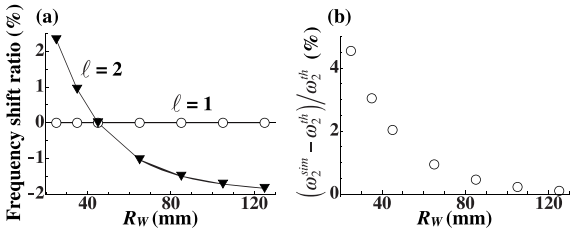

Fig. 8 Variation in the mode frequency with the position of the conducting wall R_W. (a) Frequencies of the dipole (○) and quadrupole (▼) modes for each R_W. All data points are normalized by the frequency at $R_W = 45$ mm. (b) Dependence on R_W of the ratio of the calculated frequency ω_2^{sim} to the frequency ω_2^{th} theoretically predicted using Eq. (5).

The mode frequencies calculated for variation in the wall position R_W from 25 to 125 mm are shown in Fig. 8. Figure 8 (a) shows that the quadrupole mode frequency shifts upward as the wall approaches the plasma, whereas the dipole mode frequency does not change at all. When compared to the theoretical prediction given by Eq. (5) [see Fig. 8 (b)], the quadrupole mode frequency is observed to approach the theoretical result as the conducting wall recedes from the plasma. This analysis supports the above-mentioned inference that the image charge effect causes the upward shift of the mode frequency.

5. Conclusion

In this study, we experimentally investigated the frequency characteristics of the axisymmetric eigenmodes of a spheroidal pure electron plasma. It is confirmed that the observed spheroidal plasma attains a theoretically expected equilibrium density distribution, with the exception of the case wherein a halo distribution surrounds the plasma. When the eigenmode frequency observed for the

plasma is compared with the frequency predicted by the dispersion relation, it is observed that the absolute value of the observed frequency is systematically higher than the theoretical prediction, while both frequencies show a similar dependence on the aspect ratio.

The experimental observations and numerical calculations demonstrate that the upward shift of the mode frequency cannot be accounted for solely by the finite temperature effect but is significantly affected by the image charges induced on the conducting wall. This result indicates that in order to carry out nondestructive diagnostics of plasma parameters on the basis of measurements of the eigenmode frequency, it is necessary to develop a dispersion relation that includes the effects of actual experimental conditions.

[1] D. H. E. Dubin and T. M. O'Neil, Rev. Mod. Phys. **71**, 87 (1999).
[2] D. H. E. Dubin, Phys. Rev. Lett. **66**, 2076 (1991).
[3] D. J. Heinzen, J. J. Bollinger, F. L. Moore, W. M. Itano and D. J. Wineland, Phys. Rev. Lett. **66**, 2080 (1991).
[4] C. S. Weimer, J. J. Bollinger, F. L. Moore and D. J. Wineland, Phys. Rev. A **49**, 3842 (1994).
[5] M. D. Tinkle, R. G. Greaves, C. M. Surko, R. L. Spencer and G. W. Mason, Phys. Rev. Lett. **72**, 352 (1994).
[6] H. Higaki and A. Mohri, Jpn. J. Appl. Phys., Part 1 **36**, 5300 (1997).
[7] M. Amoretti *et al*., (ATHENA Collaboration), Phys. Plasmas **10**, 3056 (2003).
[8] M. Amoretti *et al.*, (ATHENA Collaboration), Nature **419**, 456 (2002).
[9] J. Aoki, Y. Kiwamoto and Y. Kawai, Phys. Plasmas **13**, 112109 (2006).
[10] J. Aoki, Y. Kiwamoto, Y. Soga and A. Sanpei, Jpn. J. Appl. Phys. **43**, 7267 (2004).
[11] D. H. E. Dubin, Phys. Fluids B **5**, 295 (1993).
[12] B. R. Beck, J. Fajans and J. H. Malmberg, Phys. Plasmas **3**, 1250 (1996).
[13] D. Dubin, *Numerical and Analytical Methods for Scientists and Engineers Using* Mathematica (Wiley-Interscience, Hoboken, New Jersey, 2003), Sec. 7.3 (electronic version only).